# Deuteron properties of the coupled nucleon and isobar channels model

W. P. Sitarski,* P. G. Blunden,† and E. L. Lomon
*Center for Theoretical Physics, Laboratory for Nuclear Science and Department of Physics, Massachusetts Institute of Technology, Cambridge, Massachusetts 02139*
(Received 3 August 1987)

The system of NN, NΔ, ΔΔ, and NN*(1440) channels, coupled by long-range meson exchange forces and a short-range boundary condition, has been successfully applied to medium energy NN scattering. The deuteron system includes the NN($^3S_1$,$^3D_1$), ΔΔ($^3S_1$,$^3D_1$,$^7D_1$), and NN*($^3S_1$) channels. The scattering data for nucleon $T_{\rm lab} < 1$ GeV put strong restrictions on the short-range parameters of the model, imposing $\sim 2\%$ total isobar content in the deuteron, but do not determine the relative strength of coupling among the isobar channels. In contrast, the deuteron elastic magnetic form factor is sensitive to the mixture of isobars. Adding meson exchange current contributions, a good fit to these data can be achieved, including a nontrivial prediction of a minimum near $q^2 = 50$ fm$^{-2}$, by a balance between ΔΔ($^3D_1$,$^7D_1$) components. Balancing ΔΔ($^3S_1$,$^7D_1$) with NN*($^3S_1$), assuming a negative N* isoscalar magnetic moment, is only adequate for $q^2 < 25$ fm$^{-2}$. The static properties of the deuteron are well fitted, and the electric and tensor polarization form factors are consistent with the data. The inclusion of the lowest six-quark state, with cloudy bag model dynamics, increases the boundary radius, requiring $\sim 7\%$ isobar content proportioned as above to approximately fit the data.

## I. INTRODUCTION

The static deuteron properties, including the magnetic moment $\mu_d$, the quadrupole moment $Q$, and the asymptotic $S$ and $D$ state amplitudes $A_S$ and $A_D$, impose strong restrictions on the deuteron wave function. Because they probe short distance components as a function of four-momentum transfer $q$, the elastic form factors impose even stronger requirements. The elastic form factor $A(q^2)$ probes most deeply as it is known[1] to $q^2 = 100$ fm$^{-2}$. However, the magnetic form factor $B(q^2)$ is more sensitive to the isobar components in the deuteron each of which has its characteristic spin and convective magnetic effects. It is now measured[2,3] up to $q^2 = 70$ fm$^{-2}$, which is sensitive to the range of meson and isobar components. For $q^2 < 50$ fm$^{-2}$ the form factors are not greatly dependent on higher order meson exchange current (MEC), relativistic, and free quark contributions.

It is not meaningful to fit the deuteron properties unless the nuclear force used is theoretically well based and satisfactorily fits other multinucleon phenomena, especially the two-nucleon scattering data. In particular, the sensitivity of $B(q^2)$ to isobar components implies a relationship to medium energy NN scattering as the latter is strongly affected by isobar channel thresholds for $T_{\rm lab} > 400$ MeV beam energy. To meet these criteria, we use the coupled channel NN interaction of Refs. 4 and 5. In applying the constraint of fitting all the NN data for $T_{\rm lab} < 1$ GeV the present results differ from previous inclusions of isobar components in the deuteron form factor calculations. At medium and long range the potential matrix connecting all channels includes the one-pion exchange (OPE) contributions. The $\eta$, $\rho$, $\omega$, and two-pion exchange contributions are also included in the potential of the nucleon-nucleon sector. For the transition potentials between nucleon and isobar sectors, a phenomenological two-pion range Yukawa potential is substituted for the two-pion and heavy meson contributions. This phenomenological term only contributes to elastic scattering at $\frac{1}{4}m_\pi^{-1}$ range. All relevant coupled isobar channels are considered, including NΔ, ΔΔ, and NN*(1440) systems (the NΔ channel is not coupled to the $I=0$ deuteron).

At a short range, $r_0$, a homogeneous boundary condition is imposed,

$$r_0 \left[ \frac{d\Psi}{dr} \right]_{r_0} = f\Psi(r_0) , \tag{1}$$

where $\Psi$ is the multichannel (column matrix) wave function and the symmetric $f$ matrix is a meromorphic function of energy with real poles and positive residues. This form is required by hermiticity and causality.[6] Most important from our contemporary view is that asymptotic freedom implies that $r_0$ can be chosen so that free valence quark degrees of freedom dominate interior to it. It follows that the possible quark configurations determine[7,8] the pole positions and residues of the $f$ matrix, leaving only the energy independent terms as parameters.

Such an interaction with $r_0 \approx \frac{1}{2}m_\pi^{-1}$ and with only a constant $f$ matrix has been successfully applied[4,5] to fit the complex phases of all the nucleon-nucleon partial waves for $T_{\rm lab} \leq 1$ GeV. For the above small value of $r_0$, ignoring the pole terms in the $f$ matrix is justified over this energy range because (i) the lowest six-quark states occur at $T_{\rm lab} > 3.4$ GeV and have narrow width,[8] producing negligible energy dependence for $T_{\rm lab} < 1$ GeV, and (ii) at $\frac{1}{2}m_\pi^{-1}$ the two-pion exchange forces are strongly nonlocal, which, in the limit, produces a constant $f$ matrix.[6] The first set of results presented here

 

are based on this simple choice of $f$ matrix. Preliminary results have been presented earlier.[9,10]

Another choice of $r_0$ which has had some success in fitting NN scattering data[8] is $r_0 = 1.05$ fm, determined by using cloudy bag model (CBM) dynamics in the interior. The lowest six-quark state is in the $^3S_1$ channel and occurs at a mass of 2.63 GeV/$c^2$ ($T_{\rm lab} = 1.8$ GeV) for this model. The resultant pole in the $f$ matrix produces a small six-quark component in the deuteron which has little influence on the deuteron form factor. But the larger value of $r_0$ does appreciably affect the NN scattering and the hadronic current. We present the deuteron form-factor properties of such a CBM model.

In Sec. II we review the relevant features of the impulse approximation with isobar components in the deuteron, and discuss the isoscalar MEC and nucleon electromagnetic form factors used. Section III briefly restates the form of the two-hadron interaction formalism used and its inclusion of short range quark degrees of freedom. This section presents the parameters of a range of specific models that fit the NN scattering data and which will be compared with the deuteron properties.

In Sec. IV the static deuteron properties and elastic magnetic form factor are compared with the data. The quadrupole moment and the asymptotic $S$ and $D$ state amplitudes fit well. It is shown that a fit to $\mu_d$ and $B(q^2)$ requires a balance of the $\Delta\Delta(^7D_1)$ and $\Delta\Delta(^3D_1)$ components. These $\Delta\Delta$ components have opposite signs of spin and convective magnetic contributions. Replacing the $\Delta\Delta(^3D_1)$ component by a substantial NN* component with negative isoscalar N* magnetic moment $\mu_*$ can correct the magnetic moment and improve the value of $B(q^2)$, but not adequately for $q^2 > 20$ fm$^{-2}$. A good fit to $B(q^2)$ up to $q^2 = 28$ fm$^{-2}$ predicts the now observed diffraction minimum[3] at high $q^2$. The sensitivity to the isobar components, to MEC contributions, and to the nucleon electromagnetic form factors is examined. For those models which satisfactorily fit the magnetic form factor, the electric and tensor polarization form factors are examined in Sec. V, and found to be satisfactory. It is noted that remaining ambiguities may soon be removed by tensor polarization data. Our conclusions are presented in Sec. VI.

## II. DEUTERON FORM-FACTOR FORMALISM

Below, we briefly restate the formalism detailed in Ref. 11 and elsewhere, going more extensively into terms which arise due to the presence of isobar channels in the deuteron.[12,13] Electron-deuteron elastic scattering has the general form

$$\frac{d\sigma}{d\Omega_e}(q^2,\theta_e) = \left[\frac{d\sigma}{d\Omega_e}\right]_{\rm Mott}\left[A(q^2) + B(q^2)\tan^2\frac{\theta_e}{2}\right], \tag{2}$$

where

$$A(q^2) = G_0^2(q^2) + (\tfrac{8}{9})\eta^2 G_2^2(q^2) + \tfrac{2}{3}\eta G_1^2(q^2), \tag{3}$$

$$B(q^2) = \tfrac{4}{3}\eta(1+\eta)G_1^2(q^2), \tag{4}$$

the c.m. scattering angle of the electron is $\theta_e$, $q^2$ is the square of the four-momentum transfer, and $\eta = q^2/4M_d^2$, $M_d$ being the deuteron mass. Furthermore, the tensor polarization $t_{20}$, whose experimental value is required to separate $G_0$ and $G_2$, is given by

$$t_{20}(q^2) = -\sqrt{2}\left[x(x+2) + \frac{y}{2}\right] \Big/ [1 + 2(x^2+y)], \tag{5}$$

where $x = \frac{2}{3}\eta G_2/G_0$ and

$$y = \tfrac{2}{3}\eta\left[\tfrac{1}{2} + (1+\eta)\tan^2\frac{\theta_e}{2}\right] G_1^2/G_0^2 .$$

The deuteron monopole, dipole, and quadrupole form factors $G_0$, $G_1$, and $G_2$, respectively, are determined by the deuteron one-body (impulse approximation) and two-body (MEC) currents.

### A. The impulse approximation

In the impulse approximation (IA) the baryon one-body currents are taken into account. For our representation of the deuteron, these are given by the nucleon and isobar components of the deuteron's Schrödinger wave function, smeared by the nucleon and isobar electromagnetic form factors. Our present model includes, in addition to the NN($^3S_1$, $^3D_1$) components, the $\Delta\Delta(^3S_1, ^3D_1, ^7D_1)$ and the NN*($^3S_1$) components. The N*(1440) is the next isobar in mass after the $\Delta$, and because it has quantum numbers identical to the nucleon it can couple in the NN* channel to any NN channel. The NN* threshold (2378 MeV/$c^2$) is lower than the $\Delta\Delta$ threshold (2464 MeV/$c^2$), which is the lowest available with a $\Delta$ isobar in an $I=0$ channel. This, and the broad width of the N* ($\sim$300 MeV) makes the NN* channel significant in the deuteron system, in spite of its somewhat small OPE coupling to the NN channel.

Using N, $\Delta$, and * superscripts for the NN, $\Delta\Delta$, and NN* channels, respectively, we have[11,12,13]

$$G_0^{\rm IA}(q^2) = G_E^{\rm N}C_E^{\rm N} + G_E^{\Delta}C_E^{\Delta} + G_E^{*}C_E^{*}, \tag{6}$$

$$G_1^{\rm IA}(q^2) = \frac{M_d}{M_p}(G_M^{\rm N}C_S^{\rm N} + G_M^{\Delta}C_S^{\Delta} + G_M^{*}C_S^{*} + \tfrac{1}{2}G_E^{\rm N}C_L^{\rm N} + \tfrac{1}{2}G_E^{\Delta}C_L^{\Delta} + \tfrac{1}{2}G_E^{*}C_L^{*}), \tag{7}$$

and

$$G_2^{\rm IA}(q^2) = G_E^{\rm N}C_Q^{\rm N} + C_E^{\Delta}C_Q^{\Delta} + G_E^{*}C_Q^{*}, \tag{8}$$

where $M_p$ is the proton mass, the $C$'s are the contributions of the point baryons determined by the deuteron wave function, and the $G_E$ and $G_M$ are the electric and magnetic isoscalar combinations of the baryonic form factors,

$$G^{N}_{E,M} \equiv G^{p}_{E,M} + G^{n}_{E,M} ,$$
$$G^{\Delta}_{E,M} \equiv G^{\Delta^+}_{E,M} + G^{\Delta^0}_{E,M} = G^{\Delta^{++}}_{E,M} + G^{\Delta^-}_{E,M} , \quad (9)$$
$$G^{*}_{E,M} \equiv \tfrac{1}{2}(G^{*+}_{E,M} + G^{n}_{E,M} + G^{*0}_{E,M} + G^{p}_{E,M}) .$$

Our form factors are defined with the following normalizations:

$$G_0(0)=1, \quad G_1(0)=M_d M_p^{-1}\mu_d, \quad G_2(0)=M_d^2 Q .$$

As usual,[11] with the NN($^3S_1$, $^3D_1$) wave functions $u(r)$ and $w(r)$, respectively,

$$C^{N}_{E} = \int dr\,[u^2(r)+w^2(r)]j_0(\tfrac{1}{2}qr) ,$$
$$C^{N}_{Q} = \frac{3}{\sqrt{2}\eta}\int_0^\infty dr\, w(r)[u(r)-2^{-3/2}w(r)]j_2(\tfrac{1}{2}qr) , \quad (10)$$
$$C^{N}_{S} = \int_0^\infty dr \left\{ [u^2(r)-\tfrac{1}{2}w^2(r)]j_0(\tfrac{1}{2}qr) + \frac{w(r)}{2}[2^{1/2}u(r)+w(r)]j_2(\tfrac{1}{2}qr) \right\} ,$$

and

$$C^{N}_{L} = \tfrac{3}{2}\int_0^\infty dr\, w^2(r)[j_0(\tfrac{1}{2}qr)+j_2(\tfrac{1}{2}qr)] .$$

For the isobar partial waves considered here we have[12,13]

$$C^{\Delta}_{E} = \int_0^\infty dr(u^2_\Delta + w^2_{\Delta 3} + w^2_{\Delta 7})j_0(\tfrac{1}{2}qr) ,$$
$$C^{\Delta}_{Q} = \frac{3}{\sqrt{2}\eta}\int_0^\infty dr \left[ u_\Delta w_{\Delta 3} - 2^{-3/2}w^2_{\Delta 3} - \frac{2^{-1/2}}{7}w^2_{\Delta 7} \right] j_2(\tfrac{1}{2}qr) , \quad (11)$$
$$C^{\Delta}_{S} = \int_0^\infty dr[(u^2_\Delta - \tfrac{1}{2}w^2_{\Delta 3} + 2w^2_{\Delta 7})j_0(\tfrac{1}{2}qr) + (2^{-1/2}u_\Delta w_{\Delta 3} + \tfrac{1}{2}w^2_{\Delta 3} - \tfrac{4}{7}w^2_{\Delta 7})j_2(\tfrac{1}{2}qr)] ,$$
$$C^{\Delta}_{L} = \frac{M}{M_\Delta}\int_0^\infty dr(\tfrac{3}{2}w^2_{\Delta 3} - w^2_{\Delta 7})[j_0(\tfrac{1}{2}qr)+j_2(\tfrac{1}{2}qr)] ,$$

and

$$C^{*}_{E} = C^{*}_{S} = \int_0^\infty dr\, u^2_* j_0(\tfrac{1}{2}qr) ,$$
$$C^{*}_{Q} = C^{*}_{L} = 0 , \quad (12)$$

where $M_\Delta$ is the mass of the $\Delta$ and we have introduced $u_\Delta(r)$, $w_{\Delta 3}(r)$, $w_{\Delta 7}(r)$, and $u_*(r)$ as the wave functions of the $\Delta\Delta(^3S_1, ^3D_1, ^7D_1)$ and the NN*($^3S_1$) states, respectively.

The nucleon electromagnetic form factors $G^{n}_{E,M}$ and $G^{p}_{E,M}$ that we use are described below in Sec. II B. They are consistent with the data which, except for $G^{n}_{E}$, is moderately accurate over our energy range. Because of the lack of information about the electromagnetic form factors of the isobars, we have assumed that the isoscalar combinations have the same form as that of the nucleons,

$$G^{*}_{E}(q^2) = G^{\Delta}_{E}(q^2) = G^{N}_{E}(q^2) ,$$
$$G^{\Delta}_{M}(q^2) = \frac{\mu_\Delta}{(\mu_p+\mu_n)}G^{N}_{M}(q^2) , \quad (13)$$

and

$$G^{*}_{M}(q^2) = \left[ 1 + \frac{\mu_*}{(\mu_p+\mu_n)} \right] \frac{G^{N}_{M}(q^2)}{2} .$$

We note that $G^{N}_{E}(0)=1$ and $G^{N}_{M}(0)=\mu_p+\mu_n$, so that the isobar channel charges and magnetic moments are also properly normalized. Applying Eqs. (7)–(13) at $q^2=0$, we have[14]

$$\mu^{IA}_{d} = P_S(\mu_n+\mu_p) + P_D[-\tfrac{1}{2}(\mu_n+\mu_p)+\tfrac{3}{4}] + \tfrac{1}{2}P_*(\mu_n+\mu_p+\mu_*) + P_\Delta\mu_\Delta + P_{\Delta 3}\left[ -\tfrac{1}{2}\mu_\Delta + \frac{3}{4}\frac{M}{M_\Delta} \right] + P_{\Delta 7}\left[ 2\mu_\Delta - \frac{1}{2}\frac{M}{M_\Delta} \right] \quad (14)$$

and

$$Q^{IA} = \tfrac{1}{20}\int r^2 dr(8^{1/2}uw - w^2 + 8^{1/2}u_\Delta w_{\Delta 3} - w^2_{\Delta 3} - \tfrac{2}{7}w^2_{\Delta 7}) , \quad (15)$$

where $P_S$ and $P_D$ are the proportions of NN($^3S_1$, $^3D_1$) states and the subscripts of the other $P$'s identify them as the proportions of the states as subscripted in Eqs. (11) and (12). We note that $P_S = 1 - P_D - P_* - P_\Delta - P_{\Delta 3} - P_{\Delta 7}$.

We use a fixed value $\mu_{\Delta^+} = \mu_p$ as given by the quark model,[15] which predicts that the $\Delta$ magnetic moment is equal to the $\Delta$ charge times the proton magnetic moment. This value is in agreement with the experimental evidence.[16] However, there is no experimental information on $\mu_*$ and the appropriate quark model for an N*(1440) is ambiguous (excitation of a $1S_{1/2}$ to a $2S_{1/2}$ quark state, a breathing mode of the bag, or exotic $q^4\bar{q}$ or $q^3g$ configurations?). We therefore use $\mu_*$ as a parameter determined by $\mu_d$. However, we view any model for which $|\mu^S_*| \equiv |\mu^0_* + \mu^+_*| \geq 5\ \mu_N$ as being unlikely to correspond to reality.

Other hypotheses than those of Eqs. (13) are reasonable. The $\Delta$ or N* form factors may be proportional to the proton rather than to the sum of proton and neutron form factors, for instance. We have chosen Eqs. (13) for computational simplicity.

### B. The nucleon electromagnetic form factors

We use three sets of form factors for the results shown here, all of which adequately fit the nucleonic data. For the full selection of models that fit $B(q^2)$ best, we use the results of Höhler *et al.*,[17] which embody the theoretical particle pole form. For preliminary results and as a check on the sensitivity to the choice of nucleon form factors, we use, as in "case I" of Ref. 11, the Iachello, Jackson, Lande (IJL) particle-pole fit[18] for $G^{p}_{E}$ and $G^{p}_{E}$, the dipole fit of Bartel *et al.*[19] for $G^{n}_{M}$, and the $G^{n}_{E}$ of Galster *et al.*[20]

Recently,[21] a model of nucleon electromagnetic form factors incorporating quark dynamics has predicted substantially larger $G_E^n$ and smaller $|G_M^n|$ for $q^2>5$ fm$^2$. It shall be shown that this has little effect on the optimum proportion of isobar configurations, but that it shifts the radius of asymptotic freedom, $r_0$, which best fits the form factors to the larger of the two values discussed.

### C. Meson-exchange current and relativistic corrections

In this paper we do not make any relativistic corrections other than those included in the "pair" MEC contributions. Relativistic effects to order $q^2$ due to the recoil of the deuteron are well understood[22] and are expected to dominate the corrections for $q^2<5$ fm$^{-2}$. In our work we compare our model with the static properties ($q^2=0$) for which there are no recoil contributions, and the data at $q^2>5$ fm$^{-2}$. In the latter region the deuteron recoil corrections are expected to be dominated by relativistic corrections that are not calculable without a fully relativistic expansion. Although we do not include the relativistic corrections in our results, we make some qualitative remarks about their expected effects as predicted by some relativistic deuteron calculations.[23] The error due to ignoring the relativistic contributions is expected to be smaller than the uncertainties in the MEC corrections discussed in this article.

In our work we use the same MEC contributions as in Ref. 11, i.e., the $\pi$, $\rho$, and $\omega$ pair terms and the $\rho\pi\gamma$ contribution. They are calculated for each of the models being examined, with formulas corresponding to those of Ref. 24 with a minor modification discussed in the Appendix. For some of the nucleon force models, we compare results of the above MEC calculations with that of a simple calculation which only partly takes into account the model dependence of the MEC. The shape of each MEC pair and the $\rho\pi\gamma$ term is taken from the result[13] of the Reid soft core potential modified to include coupling to the $\Delta\Delta$ channels. The model dependence is partly taken into account by normalizing each term to the $q^2=0$ value for the specific model. The required $q^2=0$ limit of each MEC diagram is given in the Appendix. These $q^2=0$ formulas do not include hadronic form factors, although they have an effect even at $q^2=0$. The effect of the hadronic form factor is particularly significant for the $\rho\pi\gamma$ MEC term because it is large and the $\rho N\bar{N}$ vertex is strongly modified. This modification is included in our numerical results. By comparing these results with the full MEC calculation, we determine the sensitivity to the model of the $q^2$ dependence of MEC.

For the hadronic couplings that occur in the MEC expansions, we use $g^2_{\pi NN}/4\pi=14.3-14.8$, $g^2_{\rho NN}/4\pi=0.522$, $\kappa_v=3.66$, $g^2_{\omega NN}/4\pi=4.69$, and $\kappa_s=-0.12$. The hadronic form factors are

$$K_{\pi NN}=(1+q^2\Lambda_\pi^{-2})^{-1}\ ,$$
$$K_{\rho NN}=K_{\omega NN}=(1+q^2\Lambda_v^{-2})^{-1}\ , \tag{16}$$

where we have used $\Lambda_\pi=1.0$ GeV and $\Lambda_v=1.44$ GeV.

We use both $g_{\rho\pi\gamma}=0.406$ and 0.56 for the $\rho\pi\gamma$ vertex to determine the sensitivity of our results to this poorly known constant.[25] At high $q^2$ the $\rho\pi\gamma$ term dominates; therefore, we also examine the sensitivity to the $q^2$ dependence of the $\rho\pi\gamma$ vertex by substituting a dipole form factor,

$$K^D_{\rho\pi\gamma}=(1+q^2\Lambda_G^{-2})^{-2}\ , \tag{17}$$

with $\Lambda_G=0.885$ GeV, for the monopole form factor of Ref. 13,

$$K^M_{\rho\pi\gamma}=(1+q^2M_\omega^{-2})^{-1}\ . \tag{18}$$

We do not include the MEC contributions from N-$\Delta$ photoconversion [see Figs. 4(c)–4(e) of Ref. 11], but such diagrams make no contribution to $B(q^2)$ and are expected to be small effects in $A(q^2)$ and $t_{20}(q^2)$.

## III. COUPLED ISOBAR CHANNEL NUCLEON-NUCLEON INTERACTION

### A. The potentials

It has been shown[26] that the Bethe-Salpeter equation can be reduced, symmetrically in the two particles, to the Schrödinger equation with an eigenvalue which is the square of the relativistic relative momentum. If each partial wave channel is designated by $i$ or $j$, we may write

$$-\frac{d^2\psi_i}{dr^2}+\frac{L_i(L_i+1)}{r^2}\psi_i+\sum_j (M_r^iM_r^j)^{1/2}V_{ij}\psi_j=K_i^2\psi_i\ , \tag{19}$$

where $L_i$ is the channel orbital angular momentum, $M_i^a, M_i^b$ the masses of baryons in channel $i$, and $W$ the barycentric energy,

$$[(M_i^a)^2+K_i^2]^{1/2}+[(M_i^b)^2+K_i^2]^{1/2}=W\ , \tag{20}$$

$$M_r^i=\frac{M_i^aM_i^b}{(M_i^a+M_i^b)}\ . \tag{21}$$

In this reduction, if $r>\frac{1}{2}m_\pi^{-1}$, then $V_{ij}$ for one-boson exchange is very close to the usual local Yukawa form, and $V_{ij}$, for two-boson exchange, has a well-defined, nearly local form.

The Feshbach-Lomon potential[27] used in the NN sector is constructed from $\pi$, $\eta$, $\rho$, $\omega$, and $2\pi$ exchange. For the $2\pi$ exchange term, an expansion in intermediate state recoil momentum was used, resulting in two parametrized ambiguities. The two parameters were fitted to the data for $T_{\rm lab}<400$ MeV and resulted in a potential close to those given by the relativistic descriptions obtained from perturbation or dispersion theory.[26,28] As in Refs. 4 and 5, we do not vary the parameter of this potential from those of Ref. 27, other than a variation in $g^2_{\pi NN}$ of less than 3% (within the uncertainty of this constant) to fine tune the deuteron quadrupole moment and the relation between the deuteron binding energy and the triplet scattering length.

The one-pion exchange part of the transition potentials between nucleon and isobar channels is given by in-

dependently determined coupling constants as described in Ref. 4. The resulting potential matrix elements for the channels we consider are

$$
\begin{aligned}
&V_\pi[\mathrm{NN}(^3S_1)\text{-}\Delta\Delta(^3S_1)]=0.174 m_\pi V_0(m_\pi r)\ ,\\
&V_\pi[\mathrm{NN}(^3D_1)\text{-}\Delta\Delta(^3S_1)]=-0.05 m_\pi V_2(m_\pi r)\ ,\\
&V_\pi[\mathrm{NN}(^3S_1)\text{-}\Delta\Delta(^3D_1)]=-0.05 m_\pi V_2(m_\pi r)\ ,\\
&V_\pi[\mathrm{NN}(^3D_1)\text{-}\Delta\Delta(^3D_1)]=0.174 m_\pi V_0(m_\pi r)\\
&\qquad\qquad +0.035 m_\pi V_2(m_\pi r)\ ,\\
&V_\pi[\mathrm{NN}(^3S_1)\text{-}\Delta\Delta(^7D_1)]=0.276 m_\pi V_2(m_\pi r)\ ,\\
&V_\pi[\mathrm{NN}(^3D_1)\text{-}\Delta\Delta(^7D_1)]=-0.056 m_\pi V_2(m_\pi r)\ ,\\
&V_\pi[\mathrm{NN}(^3S_1)\text{-}\mathrm{NN}^*(^3S_1)]=-0.034 m_\pi V_0(m_\pi r)\ ,\\
&V_\pi[\mathrm{NN}(^3D_1)\text{-}\mathrm{NN}^*(^3S_1)]=-0.096 m_\pi V_2(m_\pi r)\ ,
\end{aligned}
\tag{22}
$$

where

$$V_0(x)=x^{-1}e^{-x}$$

and

$$V_2(x)=(x^{-1}+3x^{-2}+3x^{-3})e^{-x}\ . \tag{23}$$

In the application below, only those of the above transition potentials which connect to the explicitly named channels are included. For example, in a four-channel $\mathrm{NN}(^3S_1\text{-}^3D_1)$, $\Delta\Delta(^3S_1)$, $\mathrm{NN}^*(^3S_1)$ case the above couplings to the $\Delta\Delta(^3D_1)$ and $\Delta\Delta(^7D_1)$ channels are ignored.

In the transition potentials, the effect of the $2\pi$ continuum and $\rho$ exchange is phenomenologically represented by Yukawa forms with characteristic range of a half-pion-Compton wavelength

$$V_{2\pi}(r)=V_{2\pi}r^{-1}e^{-2m_\pi r}\ , \tag{24}$$

where the $V_{2\pi}$ constants are fitted phenomenologically.

### B. The boundary condition

In Ref. 6 it was shown that an interior boundary condition is required to be a meromorphic function of energy with real poles and positive residues to be consistent with the Wigner causality condition, unitarity, and time reversal invariance,

$$f(W)=f^0+\sum_i \frac{\rho_i}{W-W_i},\quad \mathrm{Im}W_i=0,\quad \rho_i\geq 0\ . \tag{25}$$

It was further shown that strong nonlocality within $r_0$ implies a small value of $df/dW$, indicating that the poles are above the energy range of strong nonlocality. Consideration of $2\pi$-exchange diagrams both in field theory and dispersion theory shows[6] that this condition is approached at $r\approx\frac{1}{2}m_\pi^{-1}$.

An explicit use of $R$-matrix theory in conjunction with the short-range quark structure[7] leads to the same general result, Eq. (25), with the pole positions and residues given by the complete set of internal quark states (as determined by the quark Hamiltonian and the vanishing wave function boundary condition at $r_0$). Analysis indicates[8] that the lowest $W_i$ are high enough and the $\rho_i$ small enough not to affect results in the energy range of the present application, $T_{\mathrm{lab}}<1$ GeV. However, the quantum chromodynamics (QCD) model used does affect the choice of $r_0$, and, hence, the predictions for $T_{\mathrm{lab}}<1$ GeV. For most of the models discussed below we use the Feshbach-Lomon[27] (FL) radius $r_0^{\mathrm{FL}}=0.74$ fm, as demanded by multipion exchange nonlocality and in good agreement with scattering data.[4,5,27] In this case the lowest $W_i$ is expected to be greater than 3 GeV and have a width of less than 0.1 GeV. Under these circumstances, all pole terms are effectively constant for $W<2.3$ GeV ($T_{\mathrm{lab}}<0.94$ GeV) and are incorporated in the constant term of the $f$ matrix.

Consistency with the CBM dynamics imposes a larger radius[8] $r_0^{\mathrm{CBM}}=1.05$ fm. The resulting energy dependence of the $f$ matrix still has only a minor effect on the region under discussion, but the consequences of the larger radius on NN scattering and of possible quark current effects on deuteron properties are discussed below.

### C. Models which fit the scattering data

Tables I and II list the $2\pi$-range transition potential coefficients and the $f$ matrices for six models. Model A is a four-channel fit which ignores coupling to $D$ states in the $\Delta\Delta$ channel, but includes coupling to the $\mathrm{NN}^*(^3S_1)$ state. Model B is a five-channel fit which includes the coupling to the $\Delta\Delta(^7D_1)$ channel in addition to the channels of model A. The $2\pi$-range transition potentials in the $\mathrm{NN}(^3S_1, ^3D_1)\text{-}\Delta\Delta(^7D_1)$ coupling are

TABLE I. The coefficients, $V_{2\pi}$, of the half-pion-Compton wavelength transition potentials [see Eq. (24)] for the different models. A blank indicates absence of all coupling to that channel.

| | Model | | | | | |
|---|---|---|---|---|---|---|
| | A | B | C | D | E | F |
| $\mathrm{NN}(^3S_1)\text{-}\Delta\Delta(^3S_1)$ | 3.3 | −0.2 | 0.2 | 0.0 | 0.0 | 0.0 |
| $\mathrm{NN}(^3D_1)\text{-}\Delta\Delta(^3S_1)$ | 0.2 | 0.8 | 0.4 | 0.0 | 0.0 | 0.0 |
| $\mathrm{NN}(^3S_1)\text{-}\Delta\Delta(^3D_1)$ | | | 0.4 | 0.0 | 0.0 | |
| $\mathrm{NN}(^3D_1)\text{-}\Delta\Delta(^3D_1)$ | | | 0.0 | 0.0 | 0.0 | |
| $\mathrm{NN}(^3S_1)\text{-}\Delta\Delta(^7D_1)$ | | −2.0 | −1.0 | 0.0 | 0.0 | 0.0 |
| $\mathrm{NN}(^3D_1)\text{-}\Delta\Delta(^7D_1)$ | | 0.4 | 0.3 | 0.0 | 0.0 | 0.0 |
| $\mathrm{NN}(^3S_1)\text{-}\mathrm{NN}(^3S_1)$ | −0.7 | −0.8 | | | | −6.0 |
| $\mathrm{NN}(^3D_1)\text{-}\mathrm{NN}^*(^3S_1)$ | −1.7 | 0.0 | | | | 6.0 |

TABLE II. The constant $f$-matrix components $f_{ij}^0$ [see Eq. (25)] for the different models. Models D, E, and F also have $\rho[\mathrm{NN}(^3S_1)\text{-}\mathrm{NN}(^3S_1)]=0.139$ GeV, $\rho[\mathrm{NN}(^3S_1)\text{-}\Delta\Delta(^3S_1)]=0.125$ GeV, and $\rho[\Delta\Delta(^3S_1)\text{-}\Delta\Delta(^3S_1)]=0.112\,41$ GeV, with $W_p=2.64$ GeV. The unlisted components are zero. A blank indicates absence of all couplings to that channel.

| | Model | | | | | |
|---|---|---|---|---|---|---|
| | A | B | C | D | E | F |
| $\mathrm{NN}(^3S_1)\text{-}\mathrm{NN}(^3S_1)$ | 7.9344 | 7.0328 | 15.6555 | 16.1982 | 16.1419 | 47.7693 |
| $\mathrm{NN}(^3S_1)\text{-}\mathrm{NN}(^3D_1)$ | 1.5 | 1.6 | −0.97 | 2.06 | 2.06 | −4.4 |
| $\mathrm{NN}(^3D_1)\text{-}\mathrm{NN}(^3D_1)$ | 2.5 | 1.1 | −0.1 | 1.5 | 1.5 | 2.3 |
| $\mathrm{NN}(^3S_1)\text{-}\Delta\Delta(^3S_1)$ | 1.5 | 0.0 | 0.0 | 0.0 | 0.0 | 0.0 |
| $\mathrm{NN}(^3D_1)\text{-}\Delta\Delta(^3S_1)$ | 0.0 | 0.0 | 0.0 | 0.0 | 0.0 | 0.0 |
| $\Delta\Delta(^3S_1)\text{-}\Delta\Delta(^3S_1)$ | 3.5 | 3.0 | 3.0 | 1.0 | 1.0 | 0.3 |
| $\mathrm{NN}(^3S_1)\text{-}\Delta\Delta(^3D_1)$ | | | −9.5 | −6.34 | −6.375 | |
| $\mathrm{NN}(^3D_1)\text{-}\Delta\Delta(^3D_1)$ | | | 0.0 | −1.78 | −1.788 | |
| $\Delta\Delta(^3D_1)\text{-}\Delta\Delta(^3D_1)$ | | | 4.0 | −0.8 | −0.8 | |
| $\mathrm{NN}(^3S_1)\text{-}\Delta\Delta(^7D_1)$ | | 0.0 | 0.0 | 2.7 | 2.62 | 0.0 |
| $\mathrm{NN}(^3D_1)\text{-}\Delta\Delta(^7D_1)$ | | 0.0 | 0.0 | 0.46 | 0.425 | 0.0 |
| $\Delta\Delta(^7D_1)\text{-}\Delta\Delta(^7D_1)$ | | 2.0 | 2.0 | −0.8 | −0.8 | 2.5 |
| $\mathrm{NN}(^3S_1)\text{-}\mathrm{NN}^*(^3S_1)$ | −5.4 | −5.6 | | | | −11.6 |
| $\mathrm{NN}(^3D_1)\text{-}\mathrm{NN}^*(^3S_1)$ | 0.0 | −0.7 | | | | −1.05 |
| $\mathrm{NN}^*(^3S_1)\text{-}\mathrm{NN}^*(^3S_1)$ | 3.5 | 4.0 | | | | 1.0 |

chosen to cancel much of the strong OPE term. We will see that the resulting 0.5% $\Delta\Delta(^7D_1)$ destroys the fit to $B(q^2)$ for $q^2>20$ fm$^{-2}$ in spite of the NN* channel contribution. Model C disregards coupling to the NN* channel, but includes coupling to the $\Delta\Delta(^3D_1)$ channel in the proportion needed to obtain good $B(q^2)$ properties. All of the above models have a boundary radius of $r_0=0.74$ fm.

Models D and E possess the same channels and OPE transition potentials of model C, but have the CBM value[8] of $r_0=1.05$ fm. In model D the proportion of coupling to the $\Delta\Delta(^7D_1)$ and $\Delta\Delta(^3D_1)$ states is adjusted to optimize the fit to $B(q^2)$, while model E shows just how sensitive the result is to small changes in that ratio. We note that $V_{2\pi}$ potentials coupling NN and $\Delta\Delta$ are not needed in these cases as the larger $r_0$ sufficiently reduces the OPE contribution to the transition potentials. Model F employs the same channels as model B, allowing for variation in $\mu_*$, but retains $r_0=r_0^{\mathrm{CBM}}$.

The deuteron binding energy is largely determined by the triplet scattering length, but is also affected, though less strongly, by the triplet effective range. The latter is, in turn, mostly determined by the NN OPE potential. For each model the value of $f^0_{\mathrm{NN}(^3S_1),\,\mathrm{NN}(^3S_1)}$ is chosen to fit the binding energy (BE) (which, because of its experimental accuracy, is the tightest constraint). The scattering length $a_t$ automatically assumes a number close to its experimental value because of the well-known correct behavior of the OPE. Any discrepancy can be removed by a variation of $g_{\pi\mathrm{NN}}$ of less than ±2%, well within its experimental uncertainty.[29]

Table III shows the $g_{\pi\mathrm{NN}}$, BE, $a_t$, and the percentage of each channel component in each of the six models. The binding energy may deviate by ±0.0002 MeV from the experimental value, but this is due only to the re-

TABLE III. The $\pi$NN coupling constant, the $^3S_1$ scattering length, and deuteron static properties for each model. When the NN* channel is coupled, $\mu_*$ is listed.

| | Model | | | | | | |
|---|---|---|---|---|---|---|---|
| | A | B | C | D | E | F | Expt. |
| $g^2_{\pi\mathrm{NN}}/4\pi$ | 14.3 | 14.6 | 14.8 | 14.8 | 14.8 | 14.6 | 13.5–15.0 |
| BE (MeV) | 2.2246 | 2.2248 | 2.2247 | 2.2248 | 2.2245 | 2.2245 | 2.2246 |
| $A_t$ (fm) | 5.43 | 5.43 | 5.44 | 5.44 | 5.44 | 5.47 | 5.42±0.007[a] |
| $P_D$ (%) | 5.29 | 5.22 | 5.93 | 5.76 | 5.75 | 6.69 | |
| $P_\Delta$ (%) | 0.73 | 0.00 | 0.00 | 0.00 | 0.00 | 0.00 | |
| $P_{\Delta 3}$ (%) | | | 0.86 | 5.00 | 5.08 | | |
| $P_{\Delta 7}$ (%) | | 0.47 | 0.63 | 2.13 | 2.05 | 0.21 | |
| $P_*$ (%) | 1.51 | 1.39 | | | | 7.78 | |
| $A_S$ (fm$^{-1/2}$) | 0.885 | 0.885 | 0.890 | 0.889 | 0.889 | 0.891 | 0.880±0.006[a] |
| $A_D/A_S$ | 0.0255 | 0.0253 | 0.0255 | 0.0256 | 0.0258 | 0.0252 | 0.0256±0.0004[b] |
| $Q^{\mathrm{IA}}$ (fm$^2$) | 0.275 | 0.274 | 0.276 | 0.275 | 0.275 | 0.275 | 0.277±0.003 |
| $\mu_{\mathrm{d}}^{\mathrm{IA}}$ ($\mu_{\mathrm{N}}$) | 0.842 | 0.842 | 0.859 | 0.854 | 0.849 | 0.842 | |
| $\mu_{\mathrm{d}}$ ($\mu_{\mathrm{N}}$) | 0.857 | 0.857 | 0.873 | 0.864 | 0.860 | 0.857 | 0.85735 |
| $\mu_*$ ($\mu_{\mathrm{N}}$) | −1.95 | −3.24 | | | | 0.67 | |

[a]Reference 29.
[b]Reference 30.

striction of the accuracy of $f^0_{\mathrm{NN}(^3S_1),\,\mathrm{NN}(^3S_1)}$ to four decimal places. Any further refinement would make no difference to any prediction except the BE itself. The value of $a_t$ is within three *systematic error* "standard deviations" of the experimental value[29] (5.419±0.009 fm), except for the uninteresting model F, and could be further improved by small variation of $g_{\pi\mathrm{NN}}$.

Figures 1 and 2 show that, given the variation among the phase shift analyses, the fits of all the models are of similar, adequate quality (model F is substantially worse for $\epsilon_1$). The lowest energy values of $\delta(^3D_2)$ are somewhat overly negative, which is probably due to a small inadequacy in the shape of the $2\pi$ Feshbach-Lomon potential. The models with $r_0 = r_0^{\mathrm{CBM}}$, especially D and E, are a better fit to $\delta(^3D_1)$ than the $r_0^{\mathrm{FL}}$ models, but the opposite is true for the fit to $\delta(^3S_1)$. In Figs. 3–7 we plot the wave function components for models A, B, C, D, and F. As expected, the isobar contributions decrease exponentially for $r > 1$ fm due to the large imaginary relative momentum in those channels.

## IV. DEUTERON STATIC PROPERTIES AND $B(q^2)$

In this section we present the deuteron static properties and the elastic magnetic form factor $B(q^2)$ for the models described above. The sensitivity of the form factor is examined in regard to the dependence on the following aspects:

(i) The coupled channel model, particularly with respect to the proportion of various isobar channels, the N*(1440) isoscalar magnetic moment, and the value of $r_0$.

(ii) The $\rho\pi\gamma$ vertex coupling constant and form factor as a measure of the uncertainty of MEC contributions.

(iii) The choice among reasonable nucleon electromagnetic form factors.

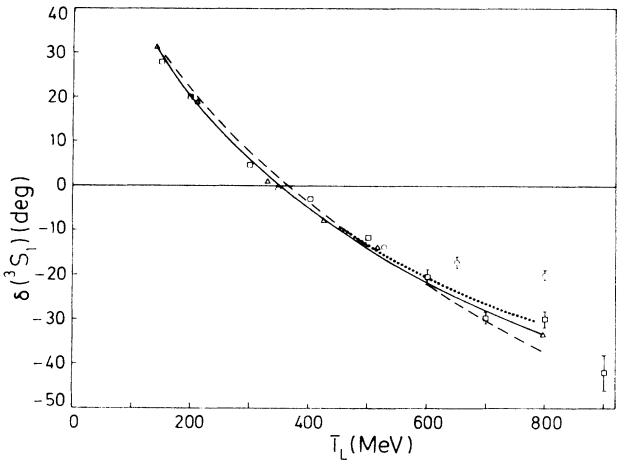


FIG. 1. The $^3S_1$ phase shift. The coupled channel model A is designated by dots, models B and C by a solid curve, and models D, E, and F by short dashes. The sources of the phase shift analysis points are denoted as in Ref. 5, using the latest results of these sources.

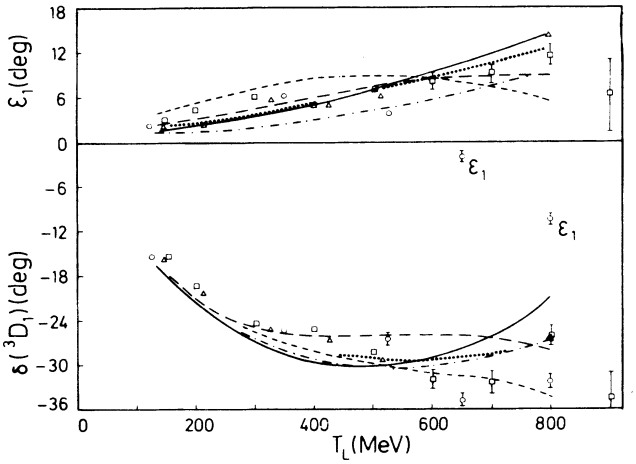


FIG. 2. The $J=1$ coupling parameter and the $^3D_1$ phase shifts for the coupled channel models. Phase shift analysis points are denoted as in Fig. 1. The dotted curve is of model A, dot-dashed of model B, solid of model C, long-dashed of models D and E, and short-dashed of model F.

### A. The static properties of the deuteron

The short-range parameters of the model are fitted to the NN scattering data and the binding energy of the deuteron. The remaining properties of the deuteron are then predicted. Table III lists for each model the values of the $S$-state asymptotic amplitude, the ratio of the $D$-state asymptotic amplitude $A_D$ to $A_S$, and the deuteron quadrupole moment in the impulse approximation, $Q^{\mathrm{IA}}$.

The experimental value is $Q^{\mathrm{expt}} = 0.2860 \pm 0.0015$ fm$^2$. As conventional MEC effects[14,24,29] are $\sim 0.007$–$0.010$ fm$^2$ for our models, one requires $Q^{\mathrm{IA}} = 0.277 \pm 0.003$ fm$^2$. $Q^{\mathrm{IA}}$ is sensitive to $g^2_{\pi\mathrm{NN}}$, which has been fine tuned in each model to produce an acceptable $Q^{\mathrm{IA}}$.

We remark here that the contributions of the isobar channels to the $Q^{\mathrm{IA}}$ [Eq. (15)] are negligible ($\sim 10^{-4}$ fm$^2$) because of the short range of the isobar channel wave functions and the $r^2$ weighting of the quadrupole integrals.

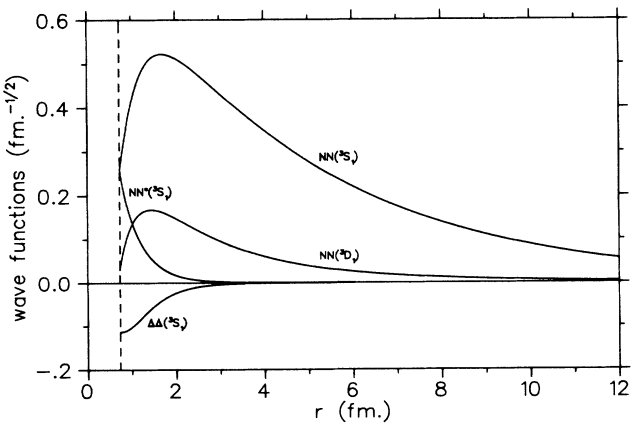


FIG. 3. The wave functions of each channel in model A. All components vanish for $r < r_0 = r_0^{\mathrm{FL}}$.

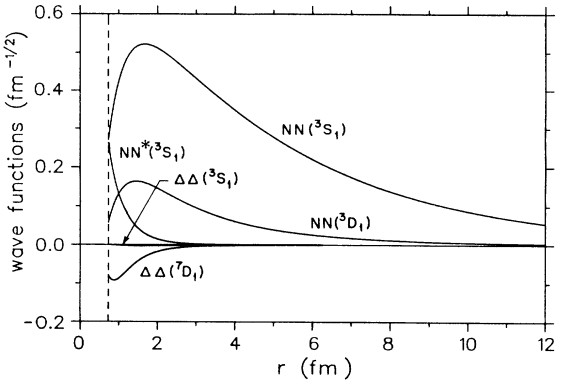


FIG. 4. The wave functions of each channel in model B. All components vanish for $r < r_0 = r_0^{\mathrm{FL}}$.

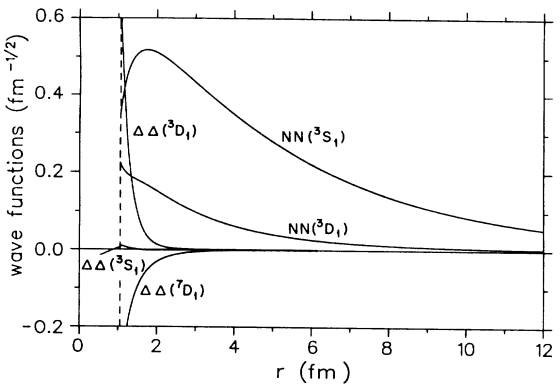


FIG. 6. The wave functions of each channel in models D or E. All hadron components vanish for $r < r_0 = r_0^{\mathrm{CBM}}$. The free quark components for $r < r_0$ are not shown, but the magnitude of their amplitude is less than 0.2.

The values of $A_S$ fall within the acceptable range of various analyses.[29] The ratios $A_D/A_S$ fall within the Coulomb stripping experimental limits of Ref. 30, and are 4–7% below the range given by the pd backward tensor polarization analysis of Ref. 31. The accuracy of the extrapolation to the $S$-matrix pole in Ref. 31 has been questioned[32] and meson exchange current effects can modify the interpretation of both experiments. For other corrections to the analysis of Ref. 30 not included in the stated $(A_D/A_S)^{\mathrm{expt}}$, see that reference.

As indicated in Fig. 8, the total two-baryon spin **S**, which determines the main part of a given channel's contribution to the deuteron magnetic moment, is aligned parallel to **J** for $^3S_1$ and $^7D_1$ states, but antiparallel to **J** for the $^3D_1$ states. This is the reason for the well-known linear decrease of $\mu_{\mathrm{d}}$ with $P_D$. But, as shown in Eq. (14), the alignment condition also determines the sign of the linear dependencies on $P_*$, $P_\Delta$, $P_{\Delta 3}$, and $P_{\Delta 7}$. [The convective terms from the $D$ states, i.e., those not proportional to magnetic moments in Eq. (14), do not contribute strongly in this region, but rather dominate at high $q^2$.] Because of the large positive value of $\mu_\Delta$ and **S** in the $\Delta\Delta(^7D_1)$ state, the effect of $P_{\Delta 7}$ is large and positive. The effect of $P_\Delta$ is also positive. As the sum of nucleon channel contributions and the MEC is already larger than $\mu_{\mathrm{d}}^{\mathrm{expt}}$, some counteracting negative contributions are required. These can only be obtained from the NN*($^3S_1$) channel if $\mu_* < 0$ or from the $\Delta\Delta(^3D_1)$ channel. Because of the relatively weak coupling of the NN* states to the nucleon system, we have not considered the effect of NN*($^3D_1$).

In Table III the magnetic moment of each model $\mu_{\mathrm{d}}^{\mathrm{IA}}$, and each model $\mu_{\mathrm{d}}$ that includes the MEC contribution, is given, along with the value of $\mu_*$ for those cases with an NN* component. Models A, B, and F have $P_* > 0.01$, resulting in a fit to $\mu_{\mathrm{d}}^{\mathrm{expt}}$ using reasonable values of $\mu_*$. In the absence of a substantial $\Delta\Delta(^3D_1)$ component, $P_{\Delta 7}$ must increase as $P_*$ decreases under the constraint of the NN elastic scattering data. In order to fit $\mu_{\mathrm{d}}$, it follows that $|\mu_*|$ must increase as $P_*^{-2}$. Consequently, for reasonable $\mu_*$ and in the absence of an important $\Delta\Delta(^3D_1)$ component, coupling to the NN* channel must be strong enough to produce near 1% of NN* or more, and coupling to the $\Delta\Delta(^7D_1)$ channel weak enough to produce $\leq 0.5\%$ in the deuteron.

In models C, D, and E, the NN* component is not coupled, but the ratio of $\Delta\Delta(^3D_1)$ to $\Delta\Delta(^7D_1)$ coupling is adjusted by the short range parameters to the best overall fit to $B(q^2)$. The resulting $\mu_{\mathrm{d}}$ is almost $\mu_{\mathrm{d}}^{\mathrm{expt}}$ for model E and is about 0.01 $\mu_{\mathrm{N}}$ too large for models C and

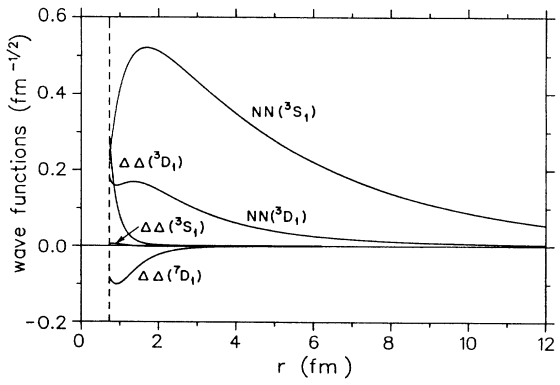


FIG. 5. The wave functions of each channel in model C. All components vanish for $r < r_0 = r_0^{\mathrm{FL}}$.

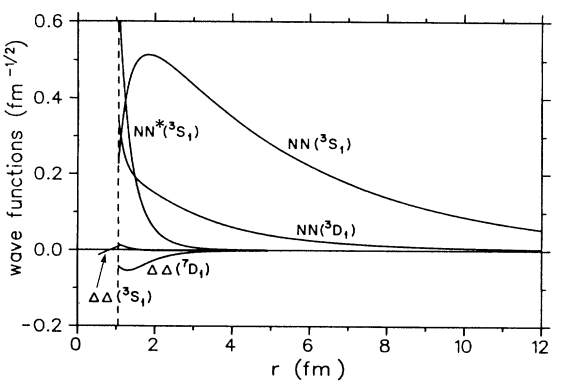


FIG. 7. The wave functions of each channel in model F. The same comments apply to $r < r_0$ as for Fig. 6.

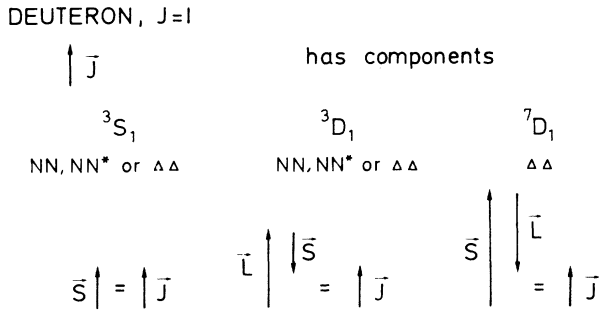


FIG. 8. The orientations of spin and orbital angular momentum of the two-hadron components of the deuteron.

D. The difference is within the range of relativistic and gradient operator (spin-orbit) corrections, both of which are negative.[14]

### B. The elastic magnetic form factor of the deuteron

Figure 9 compares the $B(q^2)$ predicted by each model with the data. $B(q^2)$ is calculated from $G_1(q^2)=G_1^{\rm IA}(q^2)+G_1^{\rm MEC}(q^2)$ using the full MEC calculation with the monopole hadronic form factors described in Sec. II with the most recent[25] experimental $g_{\rho\pi\gamma}=0.56$, and the Höhler nucleon electromagnetic form factors.[17]

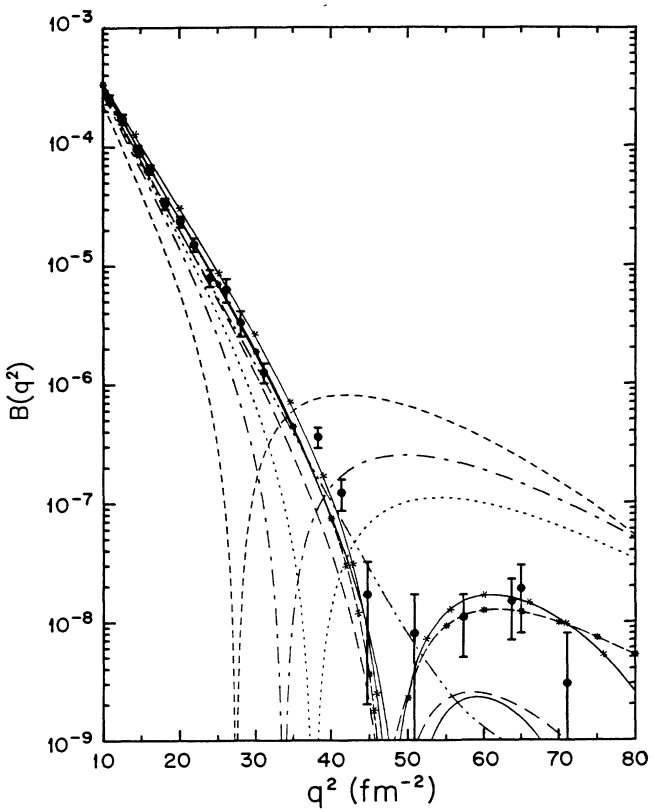


FIG. 9. The deuteron elastic magnetic form factor $B(q^2)$ for models A–F. The curve for each model is designated as in Fig. 2, except that the dashed-double-dotted curve now represents model E. The nucleon emff of Ref. 17 is used, except for curves with overlayed asterisks (*), for which those of Ref. 21 are used. All curves include the MEC contributions described in the text. The data points for $q^2<30$ fm$^{-2}$ are those of Ref. 2 and those for $q^2>30$ fm$^{-2}$ are of Ref. 3.

Model C agrees well with the Saclay data[2] over its whole energy range, while models D and E are about 30% low ($\sim$1.5 standard deviations) at the highest Saclay momentum transfer, $q^2=28$ fm$^{-2}$. It is conceivable that this deficiency in models D and E could be rectified by differences in MEC and, plausibly, as we shall see below, by an alternative set of the nucleon electromagnetic form factors (nucleon emff's) from those of Ref. 17. Model A is 50% and model B is 80% too low at this $q^2$, while model F has a diffraction minimum at $q^2=27$ fm$^{-2}$, representing isobar mixtures strongly inconsistent with the data for $q^2>8$ fm$^{-2}$. Given the uncertainties in MEC and in nucleon emff's, model A may not be a completely unsatisfactory fit to $B(q^2)$, but it lacks the physically required OPE coupling to the $\Delta\Delta(^7D_1)$ channel.

This variation in behavior can be understood in terms of the convective contributions of the isobar channels. These are present for the $L=2$ $D$ states, which because of the $j_2(\frac{1}{2}qr)$ behavior of the integrand [see $C_L^\Delta$ in Eq. (11)] dominate at high $q^2$. As shown in Fig. 8, **L** is parallel to **J** for the $\Delta\Delta(^3D_1)$ channel and antiparallel for the $\Delta\Delta(^7D_1)$ channel. It follows, as in Eq. (11), that the former channel decreases the magnitude of the negative slope of $G_1^{\rm IA}$, while the latter channel increases the magnitude. Hence, a $\Delta\Delta(^7D_1)$ component, which makes $\mu_d$ too large, tends to make $B(28\ {\rm fm}^{-2})$ too small. Model B shows that $P_{\Delta 7}<0.005$ to obtain reasonable agreement with the data when $r_0=r_0^{\rm FL}$ and the NN* channel is used to compensate for $\mu_d$. When $\Delta\Delta(^3D_1)$ is involved, and $r_0=r_0^{\rm FL}$, as in model C, we require $P_{\Delta 7}\approx 0.005$ because of the NN scattering data limitation on the total isobar content. For the $r_0=r_0^{\rm CBM}$ models with $\Delta\Delta(^3D_1)$ coupled as in models D and E, $P_{\Delta 7}\approx 0.02$ because 7% isobar content is now required by the NN scattering data to compensate for the large repulsive core. As illustrated by case F, when $r_0=r_0^{\rm CBM}$ and there is no $\Delta\Delta(^3D_1)$ contribution, no fit is possible even when $\Delta\Delta(^7D_1)$ is negligible. The large core produces a slope which is already too negative.

Of the models that fit the $q^2\leq 28$ fm$^{-2}$ data well enough (with nucleon electromagnetic form factors of Ref. 17), C and D have diffraction minima at $q^2=50$ fm$^{-2}$, while model E has no minimum and continues to decrease after $q^2=50$ fm$^{-2}$. The new data from SLAC (Ref. 3) shows a diffraction minimum or a knee near $q^2=50$ fm$^{-2}$ and a value of $(1.9\pm 1.1)\times 10^{-8}$ at $q^2=63$ fm$^{-2}$. The prediction of model C [obtained by including the constraints of OBEP and TPEP in the NN sector, OPE coupling to the isobar channels, the NN scattering data for $T_{\rm lab}<1$ GeV, and finally the $B(q^2)$ data for $q^2\leq 28$ fm$^{-2}$] is in agreement with the positions of the minimum and of the secondary maximum, but the maximum is too small. The situation is similar for model D which, however, is not fully adequate at $q^2\approx 28$ fm$^{-2}$. Model E illustrates that for $r_0=r_0^{\rm CBM}$ the position at the

minimum changes very rapidly with $P_{\Delta 7}/P_{\Delta 3}$. This is not so for $r_0 = r_0^{\mathrm{FL}}$, for which the correct prediction of the diffraction minimum is a result of the constraint of fitting $B(28\ \mathrm{fm}^{-2})$. Although not illustrated, a model for which $P_{\Delta 7}/P_{\Delta 3}$ is only 1% larger than that of model D lowers the diffraction minimum to $q^2 = 45\ \mathrm{fm}^{-2}$.

We remark that the most recent description of the neutron electromagnetic form factors[21] would increase $|G_1^{\mathrm{IA}}|$ by about 25% at $q^2 = 25\ \mathrm{fm}^{-2}$ and by about 100% at $q^2 = 60\ \mathrm{fm}^{-2}$, doubling the negative $G_1^{\mathrm{IA}}$ at the latter $q^2$. As shown in Fig. 9, this substantially improves the fit of models C and D for $q^2 > 35\ \mathrm{fm}^{-2}$. For $q^2 < 35\ \mathrm{fm}^{-2}$ it raises model C 1 to 2 standard deviations above some of the data points while increasing the values of model D to fit those data well. With these nucleon form factors, model D, and thus $r_0^{\mathrm{CBM}}$, is the best model and fits $B(q^2)$ well over the whole momentum transfer range. The other models are made worse, or are not substantially improved by these recent nucleon emff's.

In $B(q^2)$ for models D–F, we have not included any quark current contributions. If the quark amplitude was sufficiently large, this could compensate for the effect of the bigger hole in the two-baryon components due to the larger $r_0$. The $R$-matrix method provides a formula for the free quark content,[8] $P_{\mathrm{fq}}$, in $r < r_0$,

$$P_{\mathrm{fq}} = \sum_i \frac{2}{r_0 W (W - W_i)^2} [u(r_0)^2 \rho^i_{\mathrm{NN,NN}} + 2u(r_0) u_{\Delta s}(r_0) \rho^i_{\mathrm{NN},\Delta\Delta} + u^2_{\Delta s}(r_0) \rho^i_{\Delta\Delta,\Delta\Delta}] \,. \quad (26)$$

Only the lowest pole $W_1$ is treated in the models, as the higher poles have negligible influence on the energy dependence of the boundary condition in the relevant scattering region and do not affect the properties of the six-quark resonance[8] at $W_1$. The contribution of this lowest six-quark state pole to those models where $r_0 = r_0^{\mathrm{CBM}}$ is less than 0.15%, using Eq. (26).

However, as the deuteron energy $W = M_{\mathrm{n}} + M_{\mathrm{p}} - \mathrm{BE}$ is far from $W_1$, $P_{\mathrm{fq}}$ is not necessarily dominated by the lowest pole. The increasing factor $(W - W_1)^2$ in the denominator of Eq. (26) can be compensated by the large number of higher poles, whose $\rho^i$ may be somewhat enhanced. The $\rho^i$ are proportional to the product of fractional parentage coefficients for the hadronic channels, which provide a factor of 0.2 for the lowest state 1. If we assume equal spacing of states with the same quantum numbers, and an effective average fractional parentage factor of 0.5, then the higher poles will contribute $2.5 \sum_{i=2}^{\infty} i^{-2} = 1.5$ of the first pole contribution. Such a value would imply a $P_{\mathrm{fq}} = 2.5 \times 0.15\% \approx 0.4\%$. Such a value is too small to have a significant effect on the deuteron form factors. Comparison with Ref. 33, in which $P_{\mathrm{fq}} = 5\%$, shows that in our case for $q^2 \lesssim 40\ \mathrm{fm}^{-2}$ the contribution to $B(q^2)$ is less than 10% of MEC contributions. This is within the uncertainty of those MEC contributions. The quark wave function of Ref. 33 is, like ours, relativistic and massless. (Unlike ours, it has some non-$S$-wave single quark components.) A nonrelativistic, harmonic oscillator, $S$-wave quark model[34] gives a similar result for $q^2 \lesssim 40\ \mathrm{fm}^{-2}$. In future work, for precise comparison with data at $q^2 \gtrsim 40\ \mathrm{fm}^{-2}$, the quark current contribution should be included.

We comment here on the reasons why the $R$-matrix method predicts a much smaller $P_{\mathrm{fq}}$ in the deuteron than the predictions of other calculations.[33–35] In some models,[33,35] the larger value is obtained by fitting to a deuteron form factor in the absence of long range MEC contributions. In other cases,[34] it is due to the inclusion of mixed quark configurations for values of $r$ at which asymptotic freedom is not valid. These representations may be dual to our hadronic picture at such intermediate $r$. In any case, this longer range description is already taken into account in our hadronic sector. Indeed, some quark compound bag computations[36] agree with our smaller result. In our formalism, the decreased probability of entering the free-quark region, except at the energies of six-quark resonances,[8] is due to the mismatch of the 80% hidden color wave function in the interior with the color-free external wave function. The introduction of exterior hidden color components in a strongly confining potential would somewhat alter our results and should be investigated in the future.

Figure 10 demonstrates the importance of the MEC contribution and the sensitivity to $g_{\rho\pi\gamma}$. We only illustrate this for cases C and D since they are representative of the other cases with the same $r_0$. We display $G_1$ rather than $B$ because the contributions are additive in the former. It can be readily seen that MEC contributions are dominated by the impulse approximation except near the zero of the latter. The MEC contribution is very important in that it greatly increases $q^2_{\mathrm{min}}$. Nevertheless, as illustrated here, the result is qualitatively stable if the variation due to $g_{\rho\pi\gamma}$ is an indication of the MEC uncertainties. The value $g_{\rho\pi\gamma} = 0.406$ is 4.5 standard deviations less than the present value[25] of 0.56. The use of a dipole form factor at the $\rho\pi\gamma$ vertex has a somewhat larger effect if there is no correlated change in $g_{\rho\pi\gamma}$.

Figures 11 and 12 (for cases C and D, respectively) gives an indication of the sensitivity to the $q^2$ behavior of the model dependence of the MEC contribution. It compares the $q^2$ dependence of the MEC determined by the modified Reid soft core (RSC) interaction[13] scaled to the actual model results at $q^2 = 0$, with the full calculation for models C and D.

The figures also illustrate the effect of plausible variations of the nucleon emff factors. The "case 1" nucleon form factors[11] are presented with the simplified MEC contributions. (The effect of using the nucleon emff's of Ref. 21 has been shown in Fig. 9.) As shown in Fig. 11, model C with the "case 1" nucleon emff's is a very good fit at high as well as at low $q^2$. Figure 12 illustrates that these nucleon emff's make no substantial improvement for the model D fit. If future electron-nucleon experiments should validate the "case 1" nucleon emff's, then $B(q^2)$ selects model C as the best.

Figure 11 shows that the $q^2$ dependence of the RSC MEC is not very different from that of model C. But as

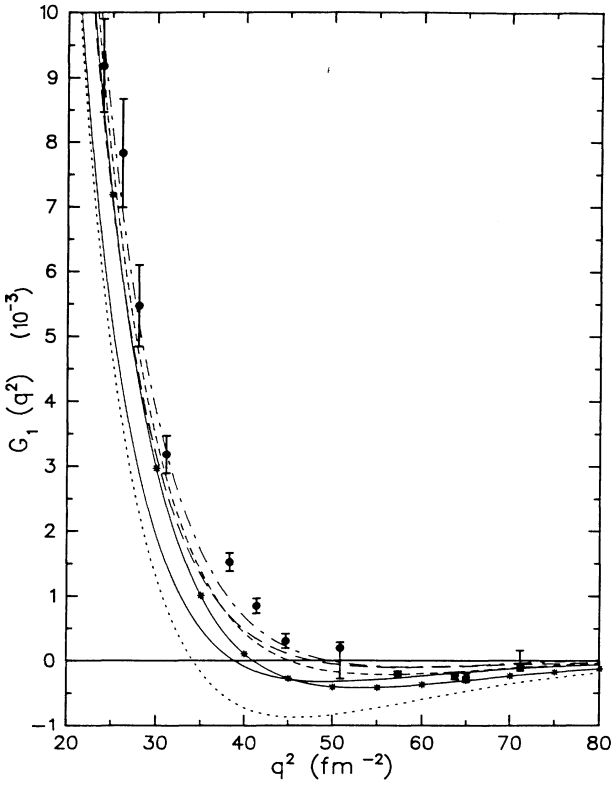


FIG. 10. The magnetic form factor amplitudes $G_1^{IA}(q^2)$ and $G_1(q^2)$ of coupled channel models C and D. All curves are obtained with nucleon emff of Ref. 17. Model C impulse approximation, dotted curve; model C total with $g_{\rho\pi\gamma}=0.56$, dash-dotted; model C total with $g_{\rho\pi\gamma}=0.406$, short dashes; model C total with $g_{\rho\pi\gamma}=0.56$ and the dipole $\rho\pi\gamma$ form factor replacing the usual monopole, solid curve with asterisks; model D impulse approximation, solid curve; and model D total with $g_{\rho\pi\gamma}=0.56$, long dashes.

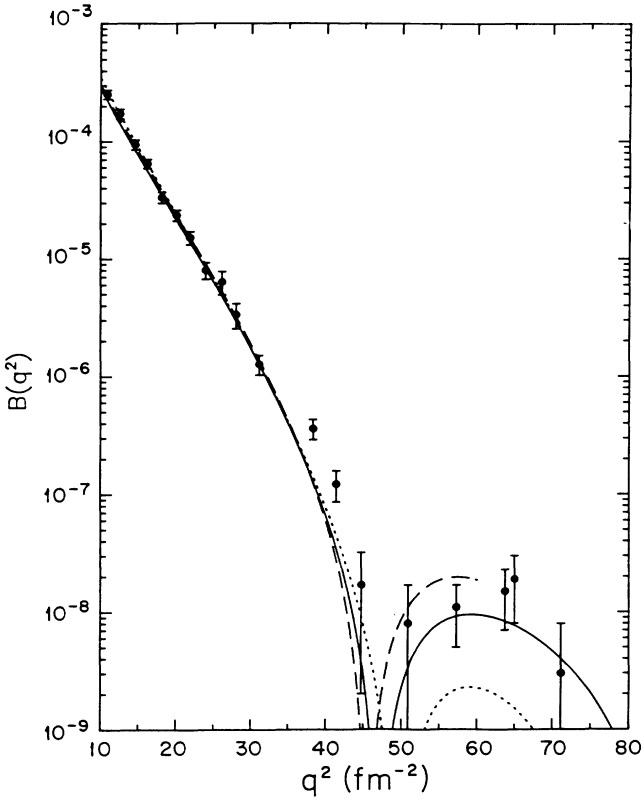


FIG. 11. $B(q^2)$ for model C. The dotted curve is obtained with the nucleon emff of Ref. 17 and the full MEC contribution described in the text. The solid curve is obtained with the same MEC, but with the "case 1" nucleon emff described in Ref. 11. The dashed curve is obtained with the "case 1" nucleon emff, but uses the approximate MEC contribution described in the text in which the model dependence is only in the normalization at $q^2=0$ and the $q^2$ dependence is that of the modified RSC model. The experimental points are denoted as in Fig. 9.

shown in Fig. 12, the large $r_0$ of model D causes a much more rapid decrease with $q$ of the size of the MEC.

Figure 13 shows that the Reid soft core and Paris potentials do not predict any minimum in $B(q^2)$ for $q^2<60$ fm$^{-2}$ when MEC contributions are included. Only in the pure impulse approximation do they agree with the new data from SLAC.[3]

## V. THE ELECTRIC FORM FACTOR AND THE TENSOR POLARIZATION

Figure 14 and 15 show that the $G_0^{IA}$ and $G_2^{IA}$ are insensitive to the proportions of isobar channels, but do depend substantially on $r_0$. Only $G_2^{IA}$ (Fig. 15) shows non-negligible sensitivity to the amount of $D$-state isobar component, which differs greatly between model F or models D or E. For $r_0=r_0^{FL}$, models A, B, and C, they are very close to the 5.2% $D$-state Feshbach-Lomon model results (model 5 of Refs. 27 and 11), where no isobar components are present.[37] However, for the $r_0^{CBM}$ models D–F, $G_0^{IA}$ is less than for the above models, changing sign at $\sim 16$ fm$^{-2}$ instead of 20 fm$^{-2}$. Also, $G_2^{IA}$ is smaller for these models, becoming negative at $q^2\approx 44$ fm$^{-2}$, and is as negative at $q^2=60$ fm$^{-2}$ as the $r_0^{FL}$ values are positive for models D and E. Figures 14 and 15 also illustrate, for model C, the substantial effect of replacing the nucleon emff of Ref. 17 with that of Ref. 21.

The MEC contributions to $G_0$ and $G_2$ are similar for all the $r_0^{FL}$ cases so that the total $A(q^2)$ and $t_{20}(q^2)$ results for all these models can be expected to resemble the 5.2% $D$-state model results of Ref. 11. However, the larger core of the $r_0^{CBM}$ models reduces the magnitude of the MEC contributions substantially. In $G_0$, the change with $r_0$ in the negative MEC contribution therefore partially compensates for the change in $G_0^{IA}$. But the decrease in $G_2^{IA}$ will be enhanced by the decrease in the positive MEC contribution.

As illustrated in Fig. 16, the effect of the larger $r_0$ on $A(q^2)$ is to decrease it everywhere, but particularly for $15<q^2<30$ fm$^{-2}$, where $G_2$ is important. When the nucleon electromagnetic form factors of Ref. 17 are used, the $r_0^{FL}$ cases fit the data[38] well, but the $r_0^{CBM}$ cases are

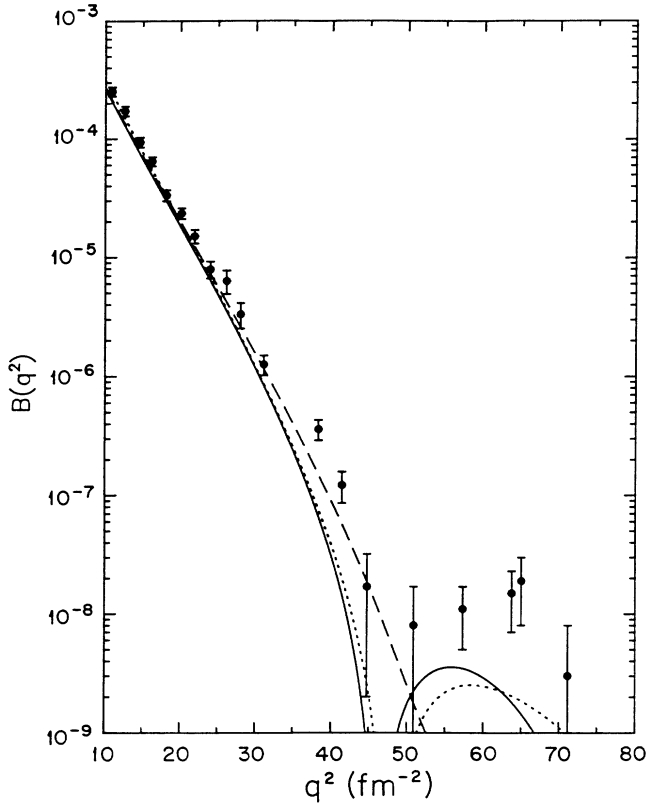


FIG. 12. The magnetic form factor $B(q^2)$ of model D. The curves have the same meaning as in Fig. 11.

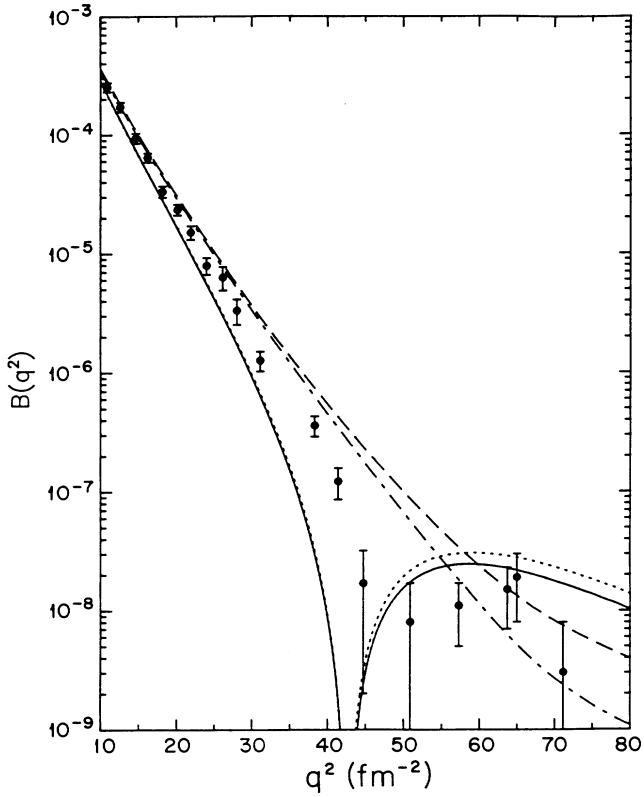


FIG. 13. $B(q^2)$ with and without MEC corrections for the Paris and RSC potentials. Paris IA, dotted; Paris total, dash-dotted; RSC IA, solid; RSC total, dashed. The experimental points are denoted as in Fig. 9.

$\sim 30\%$ too small at $q^2=28$ fm$^{-2}$. When the form factors of Ref. 21 are used, as shown for models C and D, the $r_0^{\rm FL}$ model C result is too large for $q^2>10$ fm$^{-2}$, but the $r_0^{\rm CBM}$ model D result is good for $q^2<35$ fm$^{-2}$, only becoming too large for greater $q^2$.

All the models agree with the available $t_{20}$ data,[39] which is at low $q^2=3$ and 4 fm$^{-2}$. But, as shown in Fig. 17, the $r_0^{\rm CBM}$ models predict a zero of $t_{20}$ at substantially smaller $q^2\approx 18$ fm$^{-2}$ as compared with 22 fm$^{-2}$ for the $r_0^{\rm FL}$ cases. Experiments are underway at the Bates Linac[40] that will provide values of $t_{20}$ in this $q^2$ range. At these low momentum transfers, $t_{20}$ is insensitive to the nucleon emff and uncertainties in the relativistic and meson exchange current corrections. It follows that the results of the $t_{20}$ experiment may be interpreted as an indication of the value of $r_0$, the radius of asymptotic freedom.

As shown for model C the new nucleon form factors of Ref. 21 do not make a noticeable difference to $t_{20}^{\rm IA}$ until $G_1^{\rm IA}(q^2)$ and MEC contributions become important at $q^2>50$ fm$^{-2}$, because the baryonic $G_E$ cancel in the $G_0^{\rm IA}/G_2^{\rm IA}$ ratio [see Eq. (5)].

## VI. CONCLUSIONS

The behavior of the NN elastic scattering data for $T_{\rm lab}\leq 1$ GeV requires substantial coupling to isobar channels. In the $^1D_2$ and $^3F_3$ channels this is strongly indicated by the inelastic resonances at $T_{\rm lab}=600$ and 750 MeV, respectively. However, the nonresonant $^3S_1$-$^1D_1$ channel also requires such coupling and a good fit to the data can be obtained by coupling to those $1^+$, $I=0$ channels with the lowest threshold energies. These are the $\Delta\Delta$ and NN*(1440) channels with even angular momenta. The large OPE coupling to the $\Delta\Delta(^7D_1)$ channel implies that $D$ states must be considered as well as the $S$ states for the $\Delta\Delta$ system. The coupling required by the $^3S_1$-$^3D_1$ NN scattering data results in about 1.5–7 % isobar content in the deuteron depending on $r_0$, but this data is insensitive to the proportions of the above mentioned channels.

The nonmagnetic properties of the deuteron are also relatively insensitive to the isobar distribution, and a variety of choices give good results for $A_S$, $A_D$, and $Q$ as well as the binding energy. We also have shown that models A–C (with $r_0^{\rm FL}$) all have $G_0(q^2)$ and $G_2(q^2)$ similar to that of the nonisobar models with 5.2% $D$ state[11] and are consistent with the data for $A(q^2)$ and $t_{20}(q^2)$. The $G_0$ and $G_2$ for models D–F (with $r_0^{\rm CBM}$) differ to some extent from those of the $r_0^{\rm FL}$ models, but may also be consistent with present $A$ and $t_{20}$ experiments depending on the final choices of the nucleon electromagnetic form factors, and on uncertainties in the relativistic and MEC corrections. Measurement of $t_{20}$ for

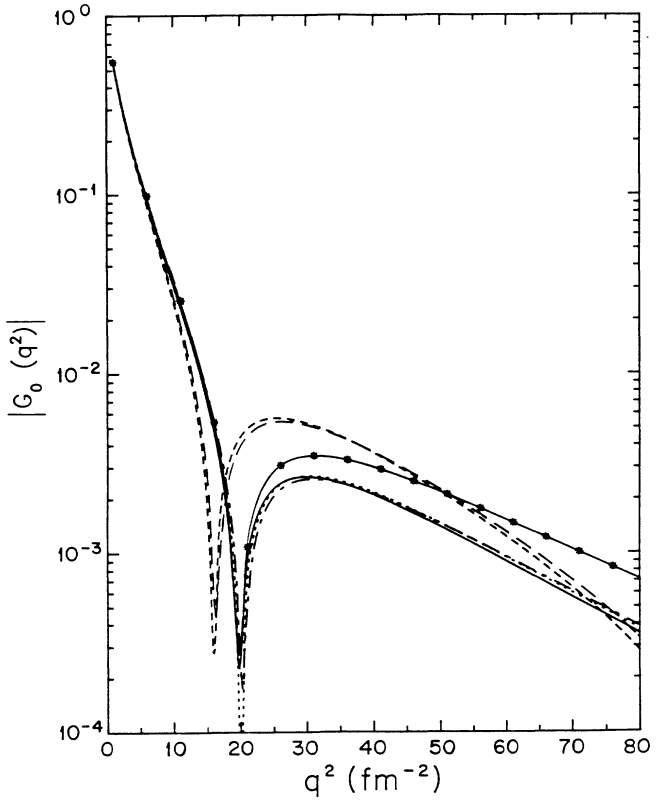


FIG. 14. The deuteron elastic monopole form factor amplitude in the impulse approximation, $G_0^{IA}(q^2)$, for models A–F. The model curves are designated as in Fig. 9, except that the model E curve is the same as the model D curve.

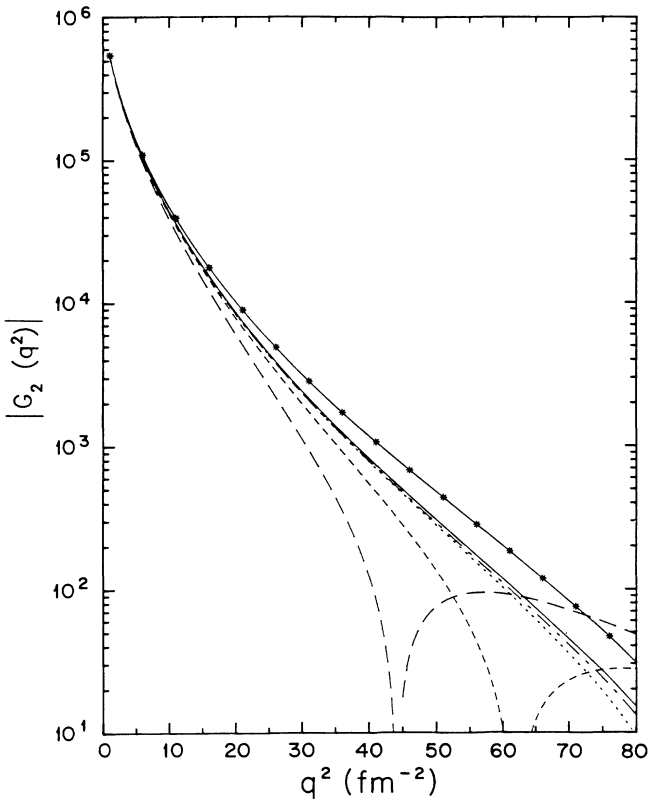


FIG. 15. The deuteron elastic quadrupole form factor amplitude in the impulse approximation, $G_2^{IA}(q^2)$, for models A–F. The model curves are designated as in Fig. 14.

$q^2 \approx 20$ fm$^{-2}$ can be expected to differentiate between the two values of $r_0$.

On the other hand, the magnetic properties $\mu_d$ and $B(q^2)$ are sensitive to the isobar magnetic moments and to the orientation of the spins and orbital angular momenta of each channel. Hence, the magnetic properties discriminate strongly among the infinite families of models that satisfy all the other constraints. We present model B as one in strong disagreement with the $B(q^2)$ data, while being in good agreement with the NN scattering data and consistent with the static properties and $A(q^2)$ and $t_{20}(q^2)$ of the deuteron. This is due to the small increase of the $\Delta\Delta(^7D_1)$ component over that in model A, as required by the OPE coupling. Any model, constrained by the NN scattering data, with more than 0.5% $\Delta\Delta(^7D_1)$ component for $r_0^{FL}$ cores (more than 2% for $r_0^{CBM}$ cores) would disagree with the $B(q^2)$. Furthermore, the value of $\mu_d$ requires a substantial coupling to either the $\Delta\Delta(^3D_1)$ or the $NN^*(^3S_1)$ channels. In the latter case the isoscalar magnetic moment is constrained to a particular, negative, value.

In the $\Delta\Delta(^7D_1)$, $NN^*(^3S_1)$ models such as A and B, $B(q^2)$ is too small for $q^2 > 25$ fm$^{-2}$ and the diffraction minimum is at a value of $q^2_{min}$ smaller than that determined by the recent SLAC data,[3] because the $NN^*(^3S_1)$ state is not as effective in reducing the slope as the $\Delta\Delta(^3D_1)$ state convective term. For the best of these models, A, plausible modification of MEC or nucleon form factors at high $q^2$ may allow a fit to the data, but the model lacks the physically required OPE coupling to the $\Delta\Delta(^7D_1)$ state.

Model C, with $r_0^{FL}$ and with the $\Delta\Delta(^3D_1)$ replacing the $NN^*(^3S_1)$ channel, includes the OPE coupling to the $^7D_1$ state. When used with the nucleon emff of Ref. 17 it fits all the data well, even better with the "case 1" nucleon emff,[11] and has the advantage of not being affected by the unknown value of $\mu_*$. In this class of model, fitting $B(q^2)$ for $q^2 \lesssim 28$ fm$^{-2}$ *predicts* the diffraction minimum at $q^2 = 50$ fm$^{-2}$.

We also investigate the effect of including quark degrees of freedom in the interior, $r > r_0$, as it results from CBM dynamics via the $R$-matrix method.[8] The main observable effects result from the increase in size of the core, $r_0$, from $r_0^{FL} = 0.74$ fm to $r_0^{CBM} = 1.05$ fm. The interior quark content is found to be $< 0.5\%$ and therefore leads to only partial compensation for the increased hole in the two-baryon wave function. The effect is to change the overall curvature of the energy dependence of the NN phase parameters and of the $q^2$ dependence of the deuteron form factors. When using the Höhler nucleon emff,[17] it results in an inadequate fit to $A(q^2)$ and $B(q^2)$. For models D and E, $A(q^2)$ is somewhat too small for $q^2 > 15$ fm$^{-2}$ and is 30% low at $q^2 = 28$ fm$^{-2}$.

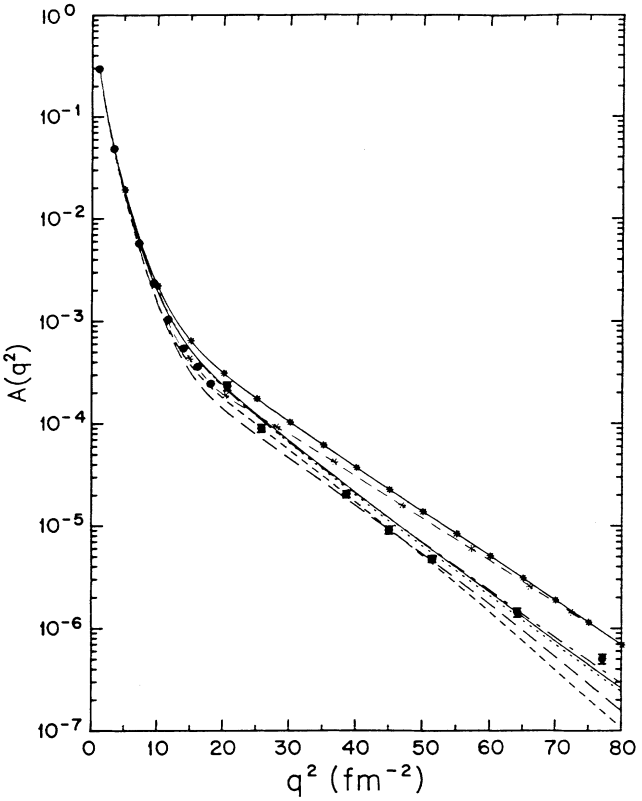


FIG. 16. The deuteron elastic electric form factor $A(q^2)$ for models A–F with the nucleon emff of Ref. 17, and for models C and D with the nucleon emff of Ref. 21. Model curves are designated as in Fig. 9 (model E is indistinguishable from model D). The data are those of Ref. 38.

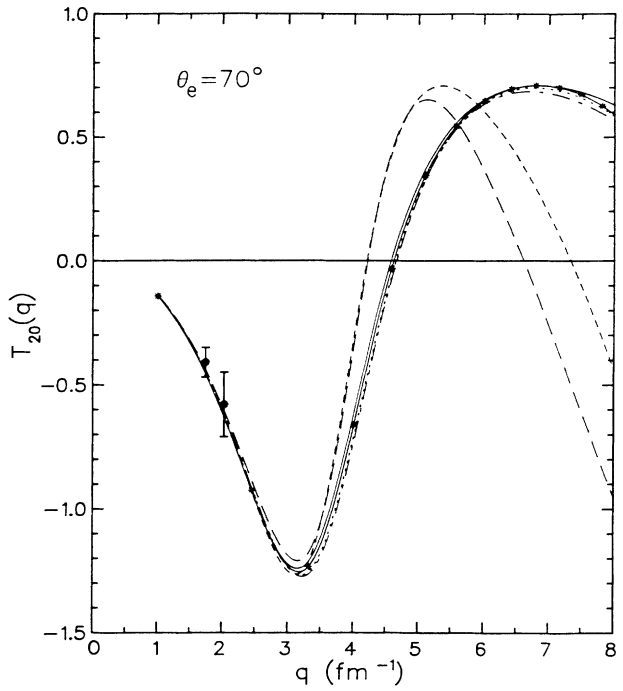


FIG. 17. The deuteron elastic tensor polarization form factor $t_{20}(q^2)$ for models A–F. The model curves are designated as in Fig. 16. The data are from Ref. 39.

For model F it is too small for $q^2 > 60$ fm$^{-2}$. With respect to $B(q^2)$, if the ratio of $\Delta\Delta(^3D_1)$ to $\Delta\Delta(^7D_1)$ is close to that required to have a diffraction minimum at $q^2 = 50$ fm$^{-2}$ as in model D, then $B(28$ fm$^{-2})$ is about 30% (2 standard deviations) too small. $B$ is very sensitive to the isobar channel ratio at $q^2 = 50$ fm$^{-2}$, but insensitive at 25 fm$^{-2}$. Consequently, a small change in that ratio, as in model E, removes the minimum to well above 70 fm$^{-2}$, but makes little improvement in $B$ at $q^2 = 28$ fm$^{-2}$.

If the Höhler nucleon form factors are replaced by the new version of Gari and Krümpelmann,[21] then the situation changes and model D fits both $A(q^2)$ and $B(q^2)$ better than does model C. Only $A(q^2)$ for $q^2 > 30$ fm$^{-2}$ does not agree with the data, and that could be corrected by a relativistic effect between that of Refs. 23(a) and 23(b). The experimental determination of $t_{20}$ near $q^2 = 20$ fm$^{-2}$ will provide important information on which of models C and D is better (and therefore on the best radius of asymptotic freedom $r_0$) because of the insensitivity of this observable to the nucleon form factors.

The $B(q^2)$ data which has recently become available[2,3] considerably improve our knowledge about the nonnucleonic structure of the deuteron. Combined with the available $A(q^2)$ data and the $t_{20}(q^2)$ data expected soon, the isobar content, radius of asymptotic freedom, and neutron form factors will be separately determined within useful limits. More theoretical study of the MEC and quark and relativistic contributions is needed to increase our confidence in the interpretation.

## ACKNOWLEDGMENTS

The authors are indebted to Drs. B. Frois, S. Platchkov, R. Arnold, and P. Bosted for early communication of experimental results. One of the authors (E.L.L.) was on leave during much of the work on this article and is grateful for the support and facilities of Continuous Elecron Beam Accelerator Facility, Newport News, VA; the Physics Division of Los Alamos National Laboratory, Los Alamos, NM; the Institut für Kernphysik, Kernforschungsanlage Julich; Institut de Physique Nucléaire, Division de Physique Théorique, Orsay, l'Université de Paris VI; and the Centre d'Etudes Recherches Nucleaires, Geneva, Switzerland. Another of us (P.G.B.) is grateful to TRIUMF, Vancouver, for its support during much of this research. This work was supported in part by funds provided by the U.S. Department of Energy (DOE) under Contract No. DE-AC02-76ER03069.

## APPENDIX

We consider the mesonic currents arising from pair terms due to $\pi$, $\rho$, and $\omega$ exchange, as well as the $\rho\pi\gamma$ exchange current. Our expressions for the two-body charge and current densities in momentum space agree with those of Gari and Hyuga (Ref. 24, Secs. 3.2 and 3.3), except that a nonlocal term in the $\rho$ exchange cor-

responding to a convection current has been included. This term was not considered previously; however, for the deuteron its overall effect is quite small.

Rather than work in momentum space, as has been done in Ref. 24, we prefer to immediately transform the current densities to coordinate space. For brevity, we present here only the expressions for $G_1(q^2)$ and only in the absence of hadronic form factors. Formulae for $G_0(q^2)$ and $G_2(q^2)$ and all the results with hadronic form factors may be obtained from one of us (P.G.B.) on request.

For the pion exchange,

$$G_1^{\pi}(q^2)=\frac{M_d}{M_p}G_M^S(q^2)\frac{g_{\pi NN}^2}{2\pi}\frac{m_\pi^2}{(2M)^3}$$
$$\times\int_0^\infty dr\{A(r)[Y_0(m_\pi r)j_0(\tfrac{1}{2}qr)+Y_2(m_\pi r)j_2(\tfrac{1}{2}qr)]$$
$$+B(r)\{Y_2(m_\pi r)j_0(\tfrac{1}{2}qr)+\tfrac{1}{2}[Y_0(m_\pi r)+Y_2(m_\pi r)]j_2(\tfrac{1}{2}qr)\}\}\ , \tag{A1}$$

while for the rho exchange,

$$G_1^{\rho}(q^2)=\frac{M_d}{M_p}F_1^S(q^2)\frac{g_{\rho NN}^2}{2\pi}\frac{m_\rho}{(2M)}\int_0^\infty dr\{(1+K_v)[A(r)-\tfrac{1}{2}B(r)](1+m_\rho r)Y_0(m_\rho r)$$
$$-\tfrac{9}{4}w^2(r)Y_0(m_\rho r)\}[j_0(\tfrac{1}{2}qr)+j_2(\tfrac{1}{2}qr)]\ . \tag{A2}$$

Here, $A(r)=u^2(r)-\frac{1}{2}w^2(r)$, $B(r)=\sqrt{2}u(r)w(r)+w^2(r)$, $Y_0(x)=e^{-x}/x$, $Y_2(x)=(1+3/x+3/x^2)Y_0(x)$, and $G_M^s(q^2)$ and $F_1^S(q^2)$ are the isoscalar magnetic and Dirac form factors, respectively. The omega exchange contribution is obtained by making the substitution $m_\rho\to m_\omega$, $K_v\to K_s$, and $g_{\rho NN}\to g_{\omega NN}$ in (A2), and multiplying by $-\frac{1}{3}$.

In the $\rho\pi\gamma$ exchange current the double propagator in the expression for the current density has been rewritten in terms of a single propagator by means of Feynman's integral. The resulting expression is

$$G_1^{\rho\pi\gamma}(q^2)=\frac{M_d}{M_\rho}K_{\rho\pi\gamma}(q^2)\frac{g_{\rho NN}g_{\pi NN}g_{\rho\pi\gamma}}{4\pi m_\rho}$$
$$\times\int_0^\infty dr\int_0^1 dz\{L(1+Lr)Y_0(Lr)[A(r)j_2(y)+B(r)j_0(y)]-(2-Lr)LY_0(Lr)A(r)j_0(y)$$
$$+\tfrac{1}{2}(2Lr-1)LY_0(Lr)B(r)j_2(y)-\tfrac{9}{10}qzLrY_0(Lr)[j_1(y)+j_3(y)]B(r)\}\ ,$$

where $L^2=m_\pi^2+(m_\rho^2-m_\pi^2)z+q^2z(1-z)$, $y=\frac{1}{2}(1-2z)qr$, and $K_{\rho\pi\gamma}(q^2)$ is the form factor at the $\rho\pi\gamma$ vertex, assumed to be given by vector meson dominance. The $q^2\to 0$ limit of the above expressions may be obtained readily. The contributions to the magnetic moment from the various terms are (in units of $e/2M$)

$$\mu(\pi\text{-pair})=\frac{g_{\pi NN}^2}{2\pi}\frac{m_\pi^2}{(2M)^3}(1+K_s)\int_0^\infty[A(r)Y_0(m_\pi r)+B(r)Y_2(m_\pi r)]dr\ ,$$
$$\mu(\rho\text{-pair})=\frac{g_{\rho NN}^2}{2\pi}\frac{m_\rho}{2M}\int_0^\infty\{(1+K_v)[A(r)-\tfrac{1}{2}B(r)](1+m_\rho r)Y_0(m_\rho r)-\tfrac{9}{4}w^2(r)Y_0(m_\rho r)\}dr\ ,$$
$$\mu(\rho\pi\gamma)=\frac{g_{\rho NN}g_{\pi NN}g_{\rho\pi\gamma}}{2\pi}\frac{1}{m_\rho(m_\rho^2-m_\pi^2)}$$
$$\times\int_0^\infty\{A(r)[m_\pi^3Y_0(m_\pi r)-m_\rho^3Y_0(m_\rho r)]+B(r)[m_\pi^3Y_2(m_\pi r)-m_\rho^3Y_2(m_\rho r)]\}dr\ .$$

*Present address: Physics Department, McGill University, Montreal, Quebec, Canada H3A 2T8.
†Present address: TRIUMF, 4004 Wesbrook Mall, Vancouver, British Columbia V6T 2A3, Canada.

[1]R. G. Arnold *et al.*, Phys. Rev. Lett. **35**, 776 (1975).
[2]S. Auffret *et al.*, Phys. Rev. Lett. **54**, 649 (1985).
[3]R. G. Arnold *et al.*, Phys. Rev. Lett. **58**, 1723 (1987).
[4]E. L. Lomon, Phys. Rev. D **26**, 576 (1982).
[5]P. González and E. L. Lomon, Phys. Rev. D **34**, 1351 (1986).
[6]H. Feshbach and E. L. Lomon, Ann. Phys. (N.Y.) **29**, 19

(1964).
[7]R. L. Jaffe and F. E. Low, Phys Rev. D **19**, 2105 (1979).
[8]E. L. Lomon, Nucl. Phys. **A434**, 139c (1985); P. LaFrance and E. I. Lomon, Phys. Rev. D **34**, 1341 (1986); P. González, P. LaFrance, and E. L. Lomon, *ibid.* **35**, 2142 (1987).
[9]E. L. Lomon, in *Proceedings of the Tenth International Conference on Few Body Problems,* Karlsruhe, 1983, edited by B. Zeitnitz (North-Holland, Amsterdam, 1985), Vol. II, p. 83.
[10]W. P. Sitarski, B.Sc. thesis, Massachusetts Institute of Technology, 1985; P. Blunden, W. P. Sitarski, and E. L. Lomon, in Proceedings of the International Nuclear Physics Conference, Harrogate, 1986, Vol. 1, p. 478; E. L. Lomon and P. Blunden, contributed paper to PANIC XI, Kyoto, 1987.
[11]E. L. Lomon, Ann. Phys. (N.Y.) **125**, 309 (1980).
[12]H. Arenhövel and H. G. Miller, Z. Phys. **266**, 13 (1974); W. Fabian, H. Arenhövel, and H. G. Miller, Z. Phys. **271**, 93 (1974).
[13]M. Gari, H. Hyuga, and B. Sommer, Phys. Rev. C **14**, 2196 (1976).
[14]E. Hadjimichael, Nucl. Phys. **A312**, 341 (1978).
[15]M. A. Bég, B. W. Lee, and A. Pais, Phys. Rev. Lett. **13**, 514 (1964).
[16]B. M. K. Nefkens *et al.*, Phys. Rev. D **18**, 3911 (1978); L. Heller, S. Kumano, J. C. Martinez, and E. J. Moniz, Phys. Rev. C **35**, 718 (1987).
[17]G. Höhler, E. Pietarinen, and I. Sabba-Stefanescu, Nucl. Phys. **B144**, 505 (1976).
[18]F. Iachello, A. D. Jackson, and A. Lande, Phys. Lett. **43B**, 191 (1973).
[19]W. Bartel *et al.*, Nucl. Phys. **B58**, 429 (1973).
[20]S. Galster *et al.*, Nucl. Phys. **B32**, 221 (1971).
[21]M. Gari and W. Krümpelmann, Z. Phys. A **322**, 689 (1985); Phys. Lett. **173B**, 10 (1986).
[22]B. M. Casper and F. Gross, Phys. Rev. **155**, 1607 (1967).
[23](a) R. G. Arnold, C. E. Carlson, and F. Gross, Phys. Rev. C **21**, 1426 (1980); (b) R. S. Bhalero and S. A. Gurvitz, *ibid.* **24**, 2773 (1981); Phys. Rev. Lett. **47**, 1815 (1981).
[24]M. Gari and H. Hyuga, Nucl. Phys. **A264**, 409 (1976).
[25]D. Berg *et al.*, Phys. Rev. Lett. **44**, 706 (1980).
[26]M. H. Partovi and E. L. Lomon, Phys. Rev. D **7**, 1999 (1970).
[27]E. L. Lomon and H. Feshbach, Ann. Phys. (N.Y.) **48**, 94 (1968).
[28]E. L. Lomon, Phys. Rev. D **14**, 2402 (1976).
[29]S. Klarsfeld, J. Martorell, and D. W. L. Sprung, J. Phys. G **10**, 165 (1984); **10**, L205 (1984); S. Klarsfeld *et al.*, Nucl. Phys. **A456**, 373 (1987).
[30]N. L. Rodning and L. D. Knutson, Phys. Rev. Lett. **57**, 2248 (1986).
[31]I. Borbély *et al.*, Phys. Lett. **109B**, 262 (1982).
[32]D. D. Pun Casavant, J. G. Sowinski, and L. D. Knutson, Phys. Lett. **154B**, 6 (1985).
[33]L. S. Kisslinger, Phys. Lett. **112B**, 307 (1982).
[34]Y. Yamauchi and W. Wakamatsu, Nucl. Phys. **A457**, 621 (1986).
[35]M. Namiki, K. Okano, and N. Oshima, Nucl. Phys. **C25**, 2157 (1982).
[36]Yu. S. Kalashnikova, I. M. Narodetskii, and A. I. Vesolov, Z. Phys. A **323**, 205 (1986).
[37]The apparently contradictory result of R. Dymarz and F. C. Khanna, Phys. Rev. Lett. **56**, 1448 (1986), may be attributable to their use of the OPE transition potential at small $r$, where the strong tensor term ($\sim r^{-3}$) can reconvert the $\Delta\Delta$ component to NN, producing the excess of NN($^1S_0$) and the nodes in the $\Delta\Delta$ function.
[38]R. G. Arnold *et al.*, Phys. Rev. Lett. **35**, 776 (1975); S. Platchkov, private communication.
[39]M. E. Shulze *et al.*, Phys. Rev. Lett. **52**, 597 (1984).
[40]R. Redwine, private communication.